Journal of Physics D:
Applied Physics

PAPER • **OPEN ACCESS**

Numerical and experimental investigation of thermal regimes of thermionic cathodes of arc plasma torches

To cite this article: M D Cunha *et al* 2023 *J. Phys. D: Appl. Phys.* **56** 395204

OPEN ACCESS
IOP Publishing
Journal of Physics D: Applied Physics
J. Phys. D: Appl. Phys. **56** (2023) 395204 (14pp)
https://doi.org/10.1088/1361-6463/ace063

Numerical and experimental investigation of thermal regimes of thermionic cathodes of arc plasma torches

M D Cunha[1,2,*], M A Sargsyan[3], M Kh Gadzhiev[3], D V Tereshonok[3] and M S Benilov[1,2]

[1] Departamento de Física, Faculdade de Ciências Exatas e da Engenharia, Universidade da Madeira, Largo do Município, 9000 Funchal, Portugal
[2] Instituto de Plasmas e Fusão Nuclear, Instituto Superior Técnico, Universidade de Lisboa, 1049-001 Lisboa, Portugal
[3] Joint Institute for High Temperatures of the Russian Academy of Sciences—Izhorskaya st. 13 Bd.2, Moscow 125412, Russia

E-mail: mario@uma.pt

Received 3 March 2023, revised 27 May 2023
Accepted for publication 21 June 2023
Published 4 July 2023

Abstract

The modelling method based on decoupling the simulation of the cathodic part of the arc (the cathode and the near-cathode non-equilibrium plasma layer) from the simulation of the arc on the whole has been extended to cathodes of arc plasma torches, consisting of an insert with a conical tip, made of pure or doped tungsten, and a surrounding water-cooled copper holder. The method was validated by comparison with the experiment, performed on a 200 A DC arc in atmospheric-pressure argon. Standard work function of polycrystalline tungsten of 4.54 eV was used for modelling of pure-tungsten insert and a good agreement with the experiment was found with respect to both the insert tip shape and the temperature distribution in the tip, recorded in the stable operation mode. There are no unambiguous data on the work function for arc cathodes made of doped tungsten, although *in situ* measurements of the effective work function of cathodes of high-pressure arc discharges provide useful hints. On the other hand, the experiments reported in this work show that the tip temperatures of inserts made of tungsten doped with 1.5% of thorium, or lanthanum, or yttrium, recorded during the stable-mode operation at the arc current of 200 A, vary in a rather narrow range 3100–3200 K. This suggests that the work functions of doped tungsten inserts, operated in the stable mode, are close to each other as well. Indeed, the results of modelling with the same value of the work function of 3 eV give a reasonably good agreement with the experiment in all three cases.

* Author to whom any correspondence should be addressed.

Keywords: numerical, experimental, investigation, thermionic cathodes, high-pressure arc discharges, deviations from local thermodynamic equilibrium

(Some figures may appear in colour only in the online journal)

1. Introduction

Adequate description of the interaction of high-pressure arcs with their electrodes remains a crucial issue to the development of predictive models of devices with high-pressure arc discharges; e.g. reviews [1–6]. In particular, an analysis of methods of modelling of the physics of interaction of high-pressure arc plasmas with thermionic cathodes is given in [6]. In many situations, current transport to cathodes of high-pressure arc discharges is governed primarily by processes in a thin near-cathode non-equilibrium plasma layer where deviations from local thermodynamic equilibrium occur, and is virtually unaffected by processes in the arc bulk; e.g. discussion in [6, section 3.3.1]. This allows one to decouple the simulation of the cathodic part of the arc (the cathode and the non-equilibrium layer) from the simulation of the arc on the whole and thus to develop a simple self-consistent approach to modelling of cathodic part of high-pressure arc discharges. This approach combines a one-dimensional description of current transport across the non-equilibrium layer and a multidimensional description of heat propagation and current flow inside the cathode. To date, this approach has undergone detailed experimental validation for thermionic rod cathodes of low-current arc discharges, used in particular in high-intensity discharge lamps (which operate at currents of no more than a few amps). One can specifically mention works of Mentel and coworkers in particular, [7]; further references can be found in [6].

Many industrial arc devices operate at much higher currents, several hundred amps or more. Cathodes of such devices are usually of complex shape with different parts made from materials with very different thermal conductivities. An example is the cathodes of high-current arc plasma torches (e.g. [8]), which often consist of a conical-tipped insert made of a thermionic material such as pure or doped tungsten, surrounded by a water-cooled copper holder.

One can hope that the modelling approach described above may be extended to such situations. Of course, it is desirable that such extension be accompanied by experimental verification. This topic is addressed in this contribution. A numerical and experimental study of cathode attachments of a 200 A DC arc in atmospheric-pressure argon is reported. Cathodes consisting of cylindrical inserts with conical tips, made of pure tungsten or tungsten doped with thorium, or yttrium, or lanthanum, surrounded by a massive water-cooled copper holder, are investigated. The computed temperature distributions closely resemble those observed in the experiment.

The outline of the paper is as follows. The experimental setup is described in section 2. The numerical model is described in section 3. Numerical and experimental results on the temperature distributions along the tips of inserts made of different materials are given and discussed in section 4. Concluding remarks are given in section 5.

2. Experiments

A fresh cathode unit as it is manufactured is illustrated by figure 1. It has a cylindrical lateral surface *DE* and a conical tip *EG*, and consists of an insert *GHIF* surrounded by a water-cooled copper holder *ABCDEFIH*. Inserts were made from different materials: pure tungsten (W), or tungsten doped with 1.5% of thorium (W_{Th}), or tungsten doped with 1.5% of yttrium (W_Y), or tungsten doped with 1.5% of lanthanum (W_{La}). The experiments were conducted on a direct current plasma torch, which consists of three modules: the cathode unit, a copper anode with an expanding channel, and a nozzle part between the cathode and the anode. The torch is described in detail elsewhere [9–11]; here we only note that the nozzle is equipped with viewing windows, which allow monitoring the state of the cathode during the operation of the torch.

Optical measurements were conducted through custom-designed viewing windows integrated into the nozzle. A clear image was projected from one of these windows using a Helios 40-2 lens onto the sensor of a high-speed, monochrome Phantom-Miro M110 camera. In contrast, from the other window, the arc image was cast (employing a quartz lens with a 220 mm focal length) onto the entry slit of a AvaSpec 2048 spectrometes, responsible for observing plasma flow emission. While operating the plasma torch at a current of 200 A and an argon flow rate of 1.5 $g\,s^{-1}$, the arc length is between 1 and 1.5 cm with a 2 mm diameter.

High-speed camera Phantom Miro M110 (capable of up to 100 000 frames s^{-1}) was used to record the cathode surface temperature, which was determined through video images captured by the same high-speed camera. Prior to use, the camera was calibrated against a reference radiation source (tungsten lamp) with a known brightness temperature, allowing it to be converted into a high-speed micropyrometer through the incorporation of an interference filter, featuring a 590 nm passband (the wave length at which there were no emission lines of plasma present) [12]. In this context, the emissivity for the solid phase of tungsten was set as 0.48 and for liquid phase (when present) was set as 0.40, as suggested by [13, 14].

The plasma in the near-cathode region was also monitored using an Avaspec 2048 spectrometer to ensure that no unexpected anomalies occurred within the plasma stream, which could inadvertently damage the cathodes in an unintended manner. Additionally, the spectrometer was employed to observe the average plasma temperature in proximity to the cathode surface.

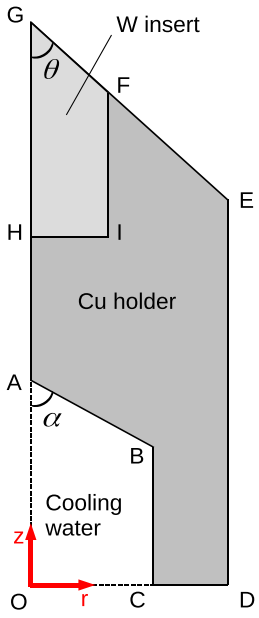

Figure 1. Schematic of a fresh cathode unit.

As far as the arc-cathode interaction is concerned, the cycle of arc operation can be divided into three stages. The initiation stage, which lasts for about 100 ms after the arcs ignition, is characterized by the ejection of microparticles and/or droplets by the cathode surface. The ejection of the microparticles can result in visible irregularities of the tip shape. An appreciable cathode erosion occurs during this stage due to the ejection of microparticles and/or droplets.

A stable arc burning mode occurs during the second stage, where the cathodic arc attachment is steady and the cathode either does not loose mass at all or looses it relatively slowly without noticeable ejection of microparticles or droplets. This stage can last up to several hours until the torch is switched off. The last one is the shutdown stage, which occurs when the power supply is switched off, provided that the power supply circuit includes a significant inductance, and is characterized by a rapid motion of the arc attachment over the cathode.

Inserts made of thoriated or lanthanated tungsten stay in the solid phase during all stages of the burning of the arc, which is a consequence of a reduction in the work function of doped tungsten. During the initiation stage, the arc attachment moves over the cathode surface in an irregular way and the loss of mass occurs due to the ejection of microparticles. There are visible irregularities on the cathode tips.

If the insert is made of pure tungsten, its tip is in a molten state throughout all stages of the arc burning. During the initiation stage, droplets are formed and ejected; a process which causes a significant erosion and is described in some detail in [15]. There is a fast change of shape of the cathode tip during the initial stage due to the droplet ejection and the motion of the molten metal in the cathode, and a much more slower variation of the tip shape at the beginning of the stable mode stage.

Inserts made of yttrated tungsten switch between solid and liquid phases at the tip during the initiation stage. Similarly to the cases of lanthanated- and thoriated-tungsten tips, the erosion occurs due to the microparticle ejection during the initial stage. During the stable operation stage, the cathode surface stays mainly in the solid phase, with occasional (for a few milliseconds in a second) shifts to the liquid phase.

All experimental data reported in this work have been acquired during the stable mode of arc burning.

3. Numerical model

3.1. Pure tungsten inserts

The approach to modelling of the cathodic part of high-pressure discharges, based on neglecting the effect of processes in the arc bulk over the cathodic part, or, in other words, on decoupling the simulation of the cathodic part of the arc from the simulation of the arc on the whole, has been developed quite some time ago and is well documented; e.g. [6, section 3.3.1] and references therein. The model used in this work is developed along the lines [16] and is described in this section.

3.1.1. Differential equations. One needs to determine distributions of the temperature T and the electrostatic potential φ in the cathode unit, i.e. in the tungsten insert and the copper water-cooled holder. According to both experiment and simulations, the insert is partially molten and the holder is in the solid state. The distributions of the temperature T and potential φ are governed by the heat conduction equation, written with account of the heat transport by the convective motion of the molten tungsten and the Joule heat generation, and by the current continuity equation combined with Ohm's law,

$$\rho c_p \frac{\partial T}{\partial t} + \rho c_p \mathbf{v} \cdot \nabla T = \nabla \cdot (\kappa \nabla T) + \sigma (\nabla \varphi)^2, \qquad (1)$$

$$\nabla \cdot (\sigma \nabla \varphi) = 0. \qquad (2)$$

Here ρ, c_p, κ, and σ are, respectively, the mass density, the specific heat, the thermal and electrical conductivities of tungsten or copper, and $\mathbf{v}$ is the velocity of the melt motion. ρ, c_p, κ, and σ, being material properties, are considered as known functions of the local temperature T, which have to be specified separately for the insert and the holder. The velocity $\mathbf{v}$ is an unknown quantity that is set to zero inside the holder and must be calculated inside the insert, and inside the solid part of the insert it must vanish. Since the time of relaxation of space charge inside metals is extremely small (of the order of 10^{-17} s for tungsten and 10^{-18} s for copper), the transient term in equation (2) is not included.

The equations (1) and (2) are solved inside the entire cathode unit, including the molten and solid parts of the insert and the holder. The account of the latent heat of melting of tungsten is introduced along the same lines as is done in simulation of metal casting [17].

The motion of the molten tungsten is described by the continuity and Navier–Stokes equations for incompressible fluid,

$$\nabla \cdot \mathbf{v} = 0, \tag{3}$$

$$\rho \frac{\partial \mathbf{v}}{\partial t} + \rho (\mathbf{v} \cdot \nabla) \mathbf{v} = \nabla \cdot \left[-p\mathbf{I} + \mu \left(\nabla \mathbf{v} + (\nabla \mathbf{v})^T \right) \right] - \sigma \nabla \varphi \times \mathbf{B}, \tag{4}$$

where p is the pressure in the melt, $\mathbf{I}$ is the identity tensor, μ is the viscosity of the melt (a known function of the temperature T), and $\mathbf{B}$ is the (self-induced) magnetic field. Note that the last term on the right-hand side of equation (4) represents the Lorentz force. The mass density of molten tungsten does not vary appreciably under conditions of this work (it decreases by about 7% as the temperature increases from 3700 K to 4300 K), which justifies the use of the approximation of incompressible fluid.

The equations (3) and (4) are solved inside the insert, including the molten and solid parts, but not in the holder. The enthalpy-porosity method [18, 19] is used for modelling the solid-liquid phase transition. Note that it is in principle possible to include also the holder in the calculation domain, however, this would be unwarranted since copper in the holder is never molten and this would only cause an unnecessary increase in the RAM requirements and the computation time.

The COMSOL Multiphysics® software is used in this work. The moving mesh functionality of the COMSOL Multiphysics® was used to explicitly track the changes in the shape of the molten tungsten surface.

3.1.2. Boundary conditions. The equations (1)–(4) are solved under the assumption of axial symmetry in the cylindrical coordinates r, z shown in figure 1. The boundary of the computation domain is similar to the one depicted by the line *ABCDEGA* in figure 1 except that the shape of the tip of the insert in the modelling is not the one of a fresh cathode, shown in figure 1: after the insert starts being melted, the position of its surface is no longer known and has to be computed.

The boundary conditions are as follows. The part of the surface of the copper holder which is in contact with the water cooling system (line *ABC* in figure 1) and the base of the holder (*CD*) are maintained at a fixed temperature T_c and the electrostatic potential here is set equal to zero:

$$ABCD: \quad T = T_c, \quad \varphi = 0. \tag{5}$$

Note that the modelling reported in this work refers to $T_c =$ 300K.

The lateral and front surfaces of the holder (*DE* and *EF*) and the front surface of the insert (*FG*) are in contact with the plasma or the cold gas and exchange energy with it. It is natural to expect, and is confirmed by the modelling, that the most of the arc current is collected by the insert. However, the possibility of current collection by the holder should not be ruled out right away. Therefore, the same boundary conditions are applied at all points of the lateral and front surfaces of the cathode unit:

$$DEG: \quad \kappa \frac{\partial T}{\partial n} = q, \quad \sigma \frac{\partial \varphi}{\partial n} = j. \tag{6}$$

Here n is a direction locally orthogonal to the cathode surface and directed outside the cathode and q and j are densities of energy flux and electric current coming from the plasma to the cathode surface. q is represented as $q = q_p - q_r$, where q_p is the density of energy flux delivered to the cathode surface by the plasma particles and q_r is the density of losses of energy by the cathode surface through radiation.

In the framework of the decoupling approach used in this work, the effect of processes in the arc bulk over the cathodic part of the arc is neglected and the densities of energy flux and electric current at the cathode surface, q_p and j, are assumed to be governed by processes in a thin near-cathode non-equilibrium layer. In the modelling of this work, these quantities are treated as known functions of T_w the local temperature of the cathode surface and U is the voltage drop across the near-cathode layer: $q_p = q_p(T_w, U)$, $j = j(T_w, U)$. U is assumed to be the same at all points of the arc attachment however varies over time. These functions have to be specified separately for the insert surface and the holder surface. A model of the near-cathode non-equilibrium plasma layer needs to be used in order to determine these functions, as discussed below.

Forces due to the surface tension and the pressure exerted by the plasma on the insert surface are introduced as boundary conditions for the Navier–Stokes equations at the surface of the insert, *FG*. The force due to surface tension is evaluated in the usual way, in terms of the curvature of the molten metal surface and the surface tension of the cathode material. The pressure p_{pl} exerted over the cathode surface by the near-cathode plasma is estimated as [16]

$$p_{\mathrm{pl}} = p_{\mathrm{amb}} + \varepsilon_0 E_w^2/2, \tag{7}$$

where ε_0 is the permittivity of free space, p_{amb} is the ambient pressure and E_w is the electric field at the cathode surface. p_{amb} was set equal to 1atm in the modelling reported in this work. E_w is treated as a known function, $E_w = E_w(T_w, U)$, which is evaluated from the model of the near-cathode non-equilibrium plasma layer jointly with the functions $q_p = q_p(T_w, U)$, $j = j(T_w, U)$. Note that the term p_{amb} in equation (7) represents the pressure exerted by the bulk plasma over the near-cathode layer, which equals the ambient pressure. The second term on the rhs describes the integral electrostatic force, applied by the electric field per unit area of the near-cathode layer.

On the cathode axis *GA*, the usual boundary conditions of axial symmetry apply. The no-slip boundary condition for the velocity is applied at the surface of contact of the insert and the holder, *FIH*.

3.1.3. Initial conditions. Both the insert and the copper holder are cold at the initial instant $t = 0$:

$$t = 0: \quad T = T_c, \quad \mathbf{v} = 0. \tag{8}$$

In principle, the model being used is capable of describing the plasma-cathode interaction at all stages of the arc burning, including the initiation stage; in particular, the droplet detachment can be simulated similarly to how it is done in

the modelling of the cathode spot formation in the vacuum arcs [20–24]. However, the simulation of detachment of a large amount of droplets is a computationally heavy task, which is not attempted in this work. The experimental value of erosion is used instead: the tip shape at $t = 0$ is assumed to be not a sharp cone shown in figure 1, but rather a truncated cone with a volume equal to the volume of the eroded tip taken from the experiment.

3.1.4. Specifying the power supply. The simplest way to specify the power supply is to specify the variation of the near-cathode voltage drop as a function of time, $U = U(t)$. After a solution has been found for a given t and the temperature distribution in the cathode unit and at the surface at this t is known, the distribution of current density over the surface for this t is evaluated in terms of the U value and the computed surface temperature distribution. Integrating the current density over the surface, one finds the arc current I value corresponding to t being considered.

Thus, if the power supply is specified in terms of the near-cathode voltage drop $U(t)$, then, after the problem (1)–(8) has been solved for the time interval desired, one will know, in particular, the variation of the arc current $I(t)$ over this time interval. On the other hand, if the modelling is aimed at simulating a particular experiment, it is more natural to specify the power supply in terms of the variation of the arc current $I(t)$: at each time, the value of U is adjusted in a way that the arc current takes a prescribed value. Then the variation of the near-cathode voltage $U(t)$ will be a computation result jointly with the temperature and potential distributions $T(r,z;t)$ and $\varphi(r,z;t)$.

In this work, the arc current time variation $I(t)$ was specified. It was implemented with the use of the 'Global equation node' option of commercial finite element software COMSOL Multiphysics®. Note that this option allows one to directly specify the discharge current without the need to introduce an equation of external electric circuit. The arc current $I(t)$ was switched from 0 to 200 A with a characteristic time of 1 ns, after which it was maintained constant and simulations progressed until a stationary solution has been attained, which includes a stationary temperature distribution in the whole cathode unit, a stationary form of the insert tip, and a stationary melt velocity field.

3.1.5. Densities of energy flux and electric current to the cathode surface. The density of energy flux delivered to the cathode surface by the plasma particles, $q_p(T_w, U)$, the density of electric current coming from the plasma to the cathode surface, $j(T_w, U)$, and the electric field at the cathode surface, $E_w = E_w(T_w, U)$, were evaluated by means of the model of non-equilibrium plasma layers at thermionic arc cathodes, summarized in [25], supplemented with an account of the secondary electron emission current. The plasma-producing gas in the near-cathode layer was assumed to be pure argon; the effect of metal vapor emitted by the cathode was not taken into account since the temperatures of the insert and holder surfaces in the experimental conditions were well below the boiling points of, respectively, tungsten and copper. Note that the electron temperature in the near-cathode layer is very high and the plasma is fully ionized, therefore the presence of a small number of metal atoms with a low ionization potential does not change appreciably the electrical and thermal conductivities of the plasma in the near-cathode layer [25].

The model [25] is designed to simulate the current transfer to hot arc cathodes, where the most of the current is transported to the cathode surface by thermionic electron emission from the surface. An account of the mechanism of current transfer to cold arc cathodes is needed to start the modelling from a cathode at room temperature. The numerical modelling [26] has shown that, after a very brief (of the order of 0.1 μs) period of arcing time, when the displacement current is the dominating mechanism, the ion current comes into play and remains the dominating mechanism until the cathode is sufficiently hot for thermionic electron emission. The supply of ionization energy into the near-cathode region, which is necessary for the generation of the ion current, is provided by the work of the sheath electric field on secondary electrons, emitted by the cathode surface due to ion impact. The effect of other potential mechanisms (field to thermo-field emission, enhancement of electric field by micro-nonuniformities on the cathode surface *etc*) is weak. In [27–29] this conclusion was supported by specially designed experiments.

Therefore, in order to develop a model suitable for multidimensional simulations of both hot and cold cathodes of high-current arc discharges, the secondary electron emission was introduced into the model of non-equilibrium plasma layers on thermionic arc cathodes, summarized in [25]. It will be shown that this modification achieves the goal and makes it possible to start the modelling from a cold cathode.

As an example, the densities of the energy flux and electric current from the atmospheric-pressure argon plasma to the surface of tungsten cathode, as well as the electric field at the cathode surface, given by the model of this work, are shown in figure 2. The solid lines have been computed with the secondary electron emission coefficient equal to 0.1; the dashed lines have been computed without account of secondary electron emission. One can see that there is a bell-shaped dependence of q_p on T_w. Without discussing this dependence in detail (e.g. [30]), we only note that the bell shape stems from a competition between the heating of the cathode surface by the ions coming from the plasma and the electron emission cooling. The electric field is sufficiently strong to produce an appreciable Schottky correction, in the range 0.3–0.6 eV. The effect of secondary electron emission is very weak for $U = 15$ and 50 V but is appreciable for $U = 150$ V in the range $T_w \lesssim 3000$ K.

The density of losses of energy by the cathode surface through radiation, $q_r(T_w)$, was evaluated in terms of temperature-dependent hemispherical total emissivity $\varepsilon(T_w)$.

3.1.6. Material properties of the cathode material. The material properties of the cathode material used in the numerical modelling were as follows. The temperature-dependent mass density $\rho(T)$, specific heat $c_p(T)$, thermal conductivity $\kappa(T)$, viscosity and surface tension of pure tungsten were taken

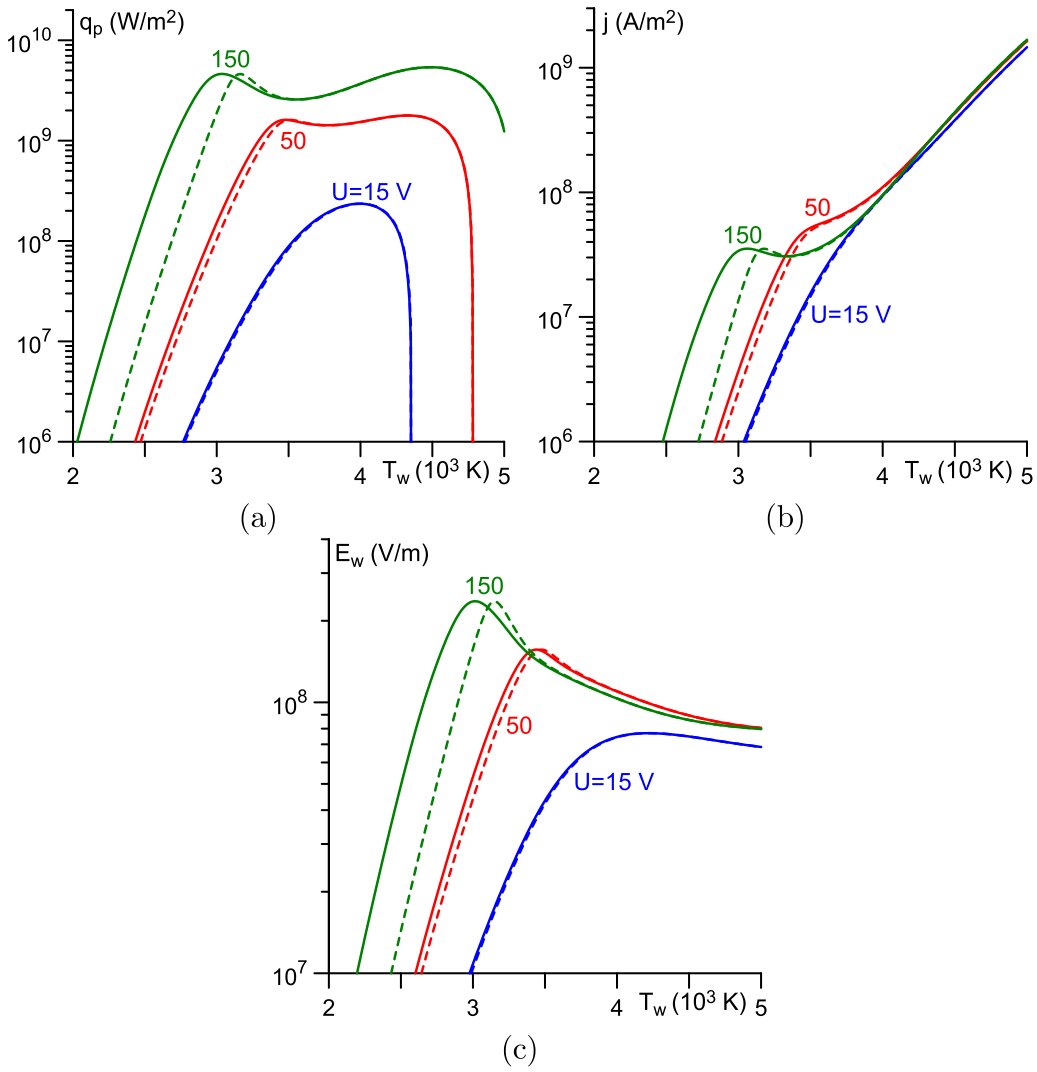

Figure 2. Computed characteristics of near-cathode plasma layer vs local cathode surface temperature for different values of the near-cathode voltage drop. Solid/dashed: calculations with and without account of secondary electron emission. Atmospheric-pressure argon plasma, tungsten cathode. (a), (b): Densities of energy flux and electric current to the cathode surface. (c): Electric field at the surface.

from [31]. The mass density, specific heat, and thermal conductivity of copper were taken from [32–34], respectively. The electrical conductivity $\sigma(T)$ of tungsten and copper was evaluated in terms of the thermal conductivity $\kappa(T)$ with the use of the Wiedemann–Franz law.

The data from [35] were used for temperature-dependent hemispherical total emissivity of tungsten. Data on the total emissivity of copper are scarce and the reported values are scattered when compared as seen in figure 3. In this work, a linear fit

$$\varepsilon = 2.2 \times 10^{-5} T_w/\mathrm{K} + 0.013 \tag{9}$$

was used.

3.2. *Inserts made of doped tungsten*

As indicated in section 2, inserts made of doped tungsten stay in the solid phase during all stages of the burning of the arc (in the case of lanthanated and thoriated tungsten), or during the most part of the stable operation stage (yttrated tungsten). Hence, there is no need in taking into account the melting of the tip material and the motion of the melt. Therefore, equations (3) and (4) with the corresponding boundary conditions are not solved in the modelling of cathodes with inserts made of doped tungsten.

Since the cathode tip shape is not computed as a part of the modelling in the framework of such approach, in contrast to the approach used for the modelling of the cathode with a pure-tungsten insert, the cathode tip shape in the stable mode has to be taken from the experiment. The microscopic images of the cathodes taken after the end of the experiment were used and irregularities of the tip shape in the images, such as deviations from the axial symmetry, were neglected. As an example, the microscopic images for inserts made of W_{Th} and W_Y are shown in figure 4 jointly with the boundaries of the calculation domain in the numerical modelling.

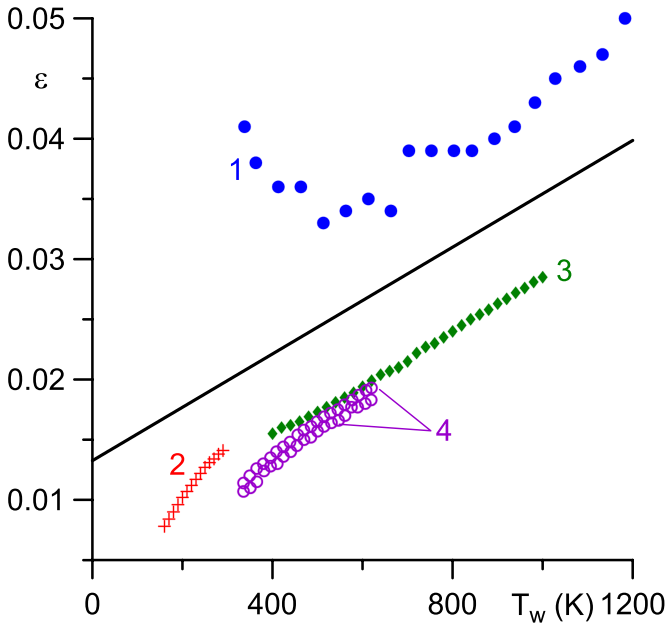

Figure 3. Experimental data and a proposed linear fit for the temperature-dependent hemispherical total emissivity of copper. Points: experimental data from [46] (1), [47] (2), [48] (3), and [49] (4). Line: the proposed linear fit, equation (9). Courtesy of Dr Helena Kaufmann.

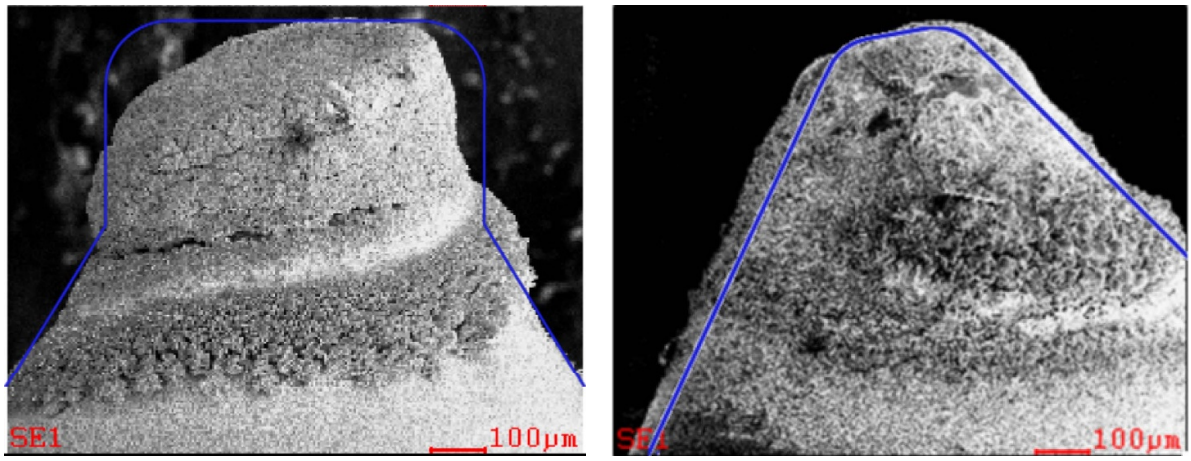

Figure 4. Microscopic images of the cathode tips after the end of the experiment. The blue lines show boundaries of the calculation domain in the numerical modelling. (a): the insert made of W_{th}. (b): the insert made of W_Y.

The material properties of pure tungsten, listed in the previous section, were used also for the doped tungsten.

3.3. Parameters governing electron emission

Important parameters governing values of the densities of the energy flux and the electric current coming from the plasma to the surface of a hot cathode, which need to be specified as input parameters for the model of near-cathode plasma layers used in this work, are the electronic work function of the cathode material, A_f, the Richardson constant (the pre-exponential factor in the Richardson–Schottky formula), A_{em}, and the secondary electron emission coefficient.

The Richardson constant is usually considered to be equal to the theoretical value $A_{em} = 1.20 \times 10^6\,\mathrm{A\,m^{-2}\,K^{-2}}$ except in early works; e.g. [36] p 6 and [37] p 135. This value is used in this work for all materials, unless otherwise specified. The secondary electron emission coefficient for all materials is set equal to 0.1.

The work function of cold surfaces of pure metals in vacuum varies depending on the state of the surface, including its crystalline structure, on the surface temperature, and on the residual gas and its pressure; e.g. [37] section 3 and [38] and references therein. In the case of thermionic cathodes of arc discharges, the variation of the work function can be expected to be much smaller due to melting or, if no melting occurs, due to high surface temperatures and the conditioning effect exerted on the cathode surface by high ion fluxes. Therefore, the standard work function of the polycrystalline metal surface is usually used in the modelling of undoped arc cathodes.

There is virtually no ambiguity in the literature regarding the work function of polycrystalline tungsten: the value of 4.54 eV is recommended in the dedicated reference book [36], values in the range (4.55 ± 0.04) eV are recommended as the most probable in the review [37], and the value of 4.55 eV is cited in the general reference book [39]. In the modelling reported in this work for the W insert, the value $A_f = 4.54$ eV is used. Values of the work function for polycrystalline copper recommended in [36, 37] are 4.40 and (4.51 ± 0.07) eV, respectively; the former value is used in this work.

For doped cathodes, the situation is much more complicated, in particular, due to the diffusion of the doping atoms in the cathode body. Therefore, there is little chance that values of the work function of cold doped metal surfaces available in the literature are applicable to arc cathodes. On the other hand, there are *in situ* measurements of effective work function of cathodes of high-pressure arc discharges [40, 41], performed by means of a technique based on the photoelectric effect and involving short laser pulses of different wavelengths focused on the cathode tip. Experiments [40] were performed in high-intensity discharge (HID) lamps. Values for the arc current are not provided, however it is known that HID lamps operate at currents of the order of one or few amps, which is consistent with the range (1–10) A mentioned in [40]. The effective work functions of (4.5 ± 0.1) eV and (3.7 ± 0.1) eV were found for, respectively, W and W_{Th} cathodes, if current transfer to the cathode occurred in the diffuse mode. The effective work functions measured in the spot mode were lower by 0.9 eV and 0.6 eV, respectively. This reduction in the effective work function was attributed to the Schottky effect occurring in the spot mode, i.e. it was assumed that the above values of 0.9 eV and 0.6 eV represent the Schottky correction in the spot mode for W and W_{Th} cathodes, respectively, while the Schottky correction in the diffuse mode is negligible.

Experiments [41] were performed on a free-burning atmospheric-pressure argon arc for the arc currents of 100 A and 200 A. Current transfer to the cathode occurred in the diffuse mode. Values of the effective work function found for cathodes made of W, W_{Th}, and W_{La} at the arc current of 200 A were, respectively, 4.6, 2.8, and 3.0 eV. Effective work functions obtained for 100 A were lower by 1.7, 0.2, and 1.0 eV, respectively. This reduction of the effective work function was attributed to the Schottky effect, as in [40], i.e. it was assumed that the above values of 1.7, 0.2, and 1.0 eV represent the Schottky correction for the arc current of 100 A for W, W_{Th}, and W_{La} cathodes, respectively, while the Schottky correction for the arc current of 200 A is negligible.

It is of interest to compare the above variations of the Schottky correction with values predicted by modelling. As an example, let us consider the measurements reported in [41] for pure W tips. The tip temperature T_w measured in [41] was 4062 and 4560 K for the arc current of 100 and 200 A, respectively. Near-cathode voltage drop is not given, but is typically around 15V in high-current arc discharges; one can make estimates for the range from 10 and 50V to be on the safe side. Using the free on-line tool for evaluation of parameters of non-equilibrium near-cathode plasma layer in high-pressure arc plasmas [42], one finds that the Schottky correction varies in this voltage range between 0.23 and 0.35 eV for $T_w = 4062$ K and between 0.26 and 0.31 eV for $T_w = 4560$ K. It follows that the reduction of the effective work function between 200 A and 100 A, estimated theoretically in terms of the measured tip temperature, does not exceed 0.09 eV. This is by a factor of 20 lower than the reduction deduced in [41]. Note that the code implemented in the tool [42] represents a module of a model of plasma-cathode interaction summarized in [25], which has gone through a detailed experimental validation for thermionic rod cathodes of low-current arc discharges; e.g. references in [6]. Of course, there is still no guarantee that this code adequately describes the experimental conditions [41], however, the Schottky correction values for thermionic arc cathodes obtained by other authors are also about 0.3 eV (e.g. [43]). It should be recognized that the variations in the Schottky correction for pure W arc cathodes deduced in [40, 41] cannot be explained theoretically, hence the results of [40, 41] should be used with caution until this point has been clarified.

Another attempt to derive the work function of thoriated-tungsten arc cathodes was undertaken in [43]. The mean current density in the cathode arc attachment was estimated in terms of the arc current and the surface temperature distribution derived from one-colour pyrometry measurements and morphological and atomic composition analyses of the cathode tips after arcing. The ion contribution to the current density was evaluated from analysis of the energy balance in the ionization zone of the near-cathode layer. The effective work function determined in this way was added by the estimated Schottky correction, which was almost constant in the range of spot temperatures of interest and approximately equal to 0.38 eV. The work function determined in this way with the Richardson constant A_{em} equal to $1.20 \times 10^6\,\mathrm{A\,m^{-2}\,K^{-2}}$ increased from 3.2 to 4.0 eV as the cathode tip temperature increased from 2900 to 3700 K. The dependence of the work function on the cathode tip temperature was attributed to the variations of the thorium coverage on the cathode surface. These results are interesting and potentially useful, although it is unclear that they can be transferred to other experimental conditions: the thorium coverage on the surface of thoriated-tungsten cathodes of high-current arcs is likely to depend not only on the surface temperature but also on the arc current, which affects the ion bombardment; and the relationship between the temperature of the cathode tip and the arc current depends on the design of the cathode and therefore varies from one experiment to another. Note that while the cathode tip temperature at the arc current of 200 A was about 3700 K in the experimental conditions [43], in the experiments of this work the thoriated-tungsten insert temperature for the arc current of 200 A was around 3200 K as discussed in the next section.

Thus, there are no unambiguous data on the work function for arc cathodes made of doped tungsten, although *in situ* measurements of the effective work function of the cathodes of high-pressure arc discharges reported in [40, 41] and the investigation of effective work function of thoriated-tungsten arc cathodes reported in [43] provide some useful indications.

Therefore, in this work, simulations were performed for various values of the work function. The specific values used for each simulation are indicated in the next section.

4. Results and discussion

Experimental results chosen for validation of the numerical modelling refer to four different cathodes of atmospheric-pressure argon arcs, operating at the current of 200 A. The inserts of the cathodes were made of four different materials: pure tungsten, lanthanated tungsten, thoriated tungsten, and tungsten doped with yttrium. The geometrical parameters of the fresh cathodes were as follows. *GH* the insert length (figure 1) was the same for all the four cathodes: $GH = 8$ mm. The geometrical parameters of the copper holder were the same as well: $GO = 35$ mm, $OC = 5$ mm, $CD = 3$ mm, $CB = 15$ mm, $\alpha = 60°$. The insert radius *HI* and the half-apex angle θ are indicated in table 1.

Temperature distributions of the cathode tip surface, recorded during the stable mode of operation of cathodes with different inserts at the arc current of 200 A are shown in figures 5(d), 6(a), 7(a) and 8(a). Note that in the case of the insert made of pure tungsten, where the tip of the insert is melted, it was observed in the experiments that the maximum temperature occurs not at the tip of the insert: a spot was observed moving along the cathode surface at about the same distance from the tip. This feature is a manifestation of 3D effects in the motion of the molten metal and is left beyond the scope of this work.

The computed evolution of the shape of the tip of the pure tungsten insert and of the temperature distribution in the tip is shown in figures 5(a)–(c). The evolution of the near-cathode voltage drop is shown in figure 9. During the first approximately 300 ms, the whole cathode surface is relatively cold and the electron emission from the cathode is mostly due to the argon ion bombardment, as is the case for conventional glow discharges. The near-cathode voltage drop U is virtually constant at 165 V. Over time, the cathode surface heats up uniformly. At 295 ms, the tip temperature is around 2100 K (figure 5(a)). A thermal instability develops around this time and an arc spot appears on the insert tip with the surface temperature in the spot exceeding 4000 K (figure 5(b)). The near-cathode voltage drop collapses to values below 20V. The tip shape starts changing due to the motion of the molten metal. The stationary regime is achieved at $t \approx 1$ s (figure 5(c)). The computed maximum tip temperature for $t = 1$ s is given in table 2 and approximately equals 4304 K. Also shown in table 2 are experimental values measured in the stable mode. As seen from table 2, the above-mentioned computed maximum steady-state temperature of the pure-tungsten insert is close to the maximum temperature measured in the stable mode, which is approximately 4200 K.

There is a small peculiarity (a cusp) in the computed cathode shape shown in figure 5(c) in the vicinity of the liquid/solid interface (we remind that the melting temperature of tungsten is 3695 K). No such peculiarity is seen in the experimental image in figure 5(d). A potential reason of this difference is the disregard of deformations of solid tungsten at temperatures slightly below the melting temperature in the numerical model. Apart from this difference, there is a good agreement between the modelling and the experiment.

It is seen from table 2 that the maximum temperatures measured in the stable mode on all inserts made of doped tungsten are rather close to each other. This suggests that the work functions of doped tungsten inserts, operated in the stable

Table 1. Geometrical parameters of inserts.

Insert material	*HI* (mm)	θ (°)
W	2	30
W_{Th}	2.5	30
W_Y	2.5	30
W_{La}	2	35

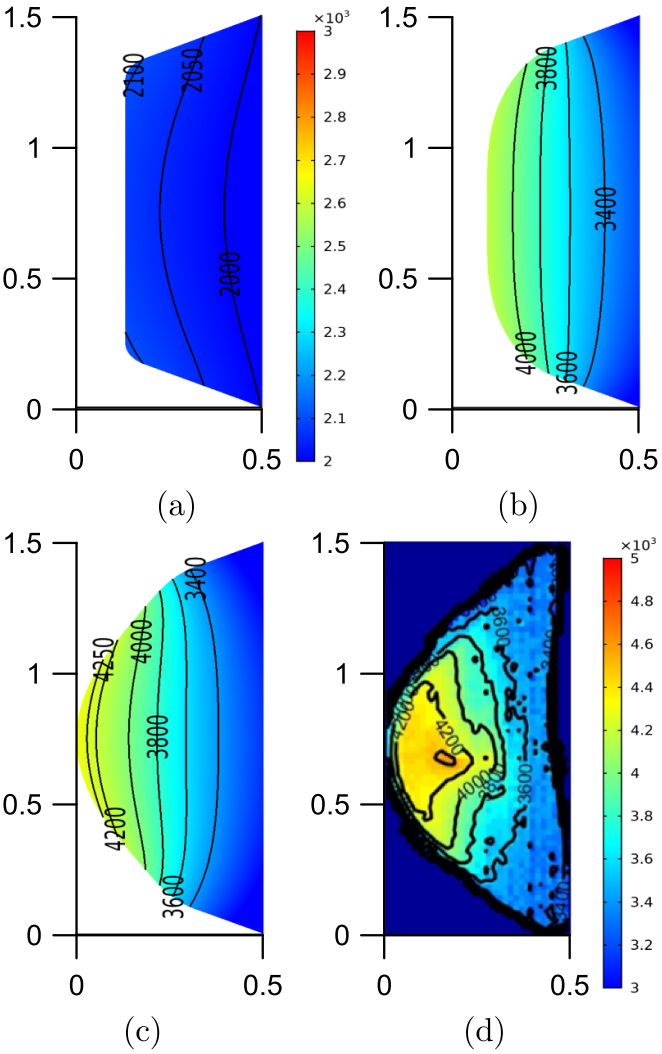

Figure 5. The cathode tip shape and the temperature distribution in the tip. (a)–(c): Modelling, $t = 295$ ms (a), 331 ms (b), 1 s (c). (d): Experiment, stable mode (Reproduced from [15]. [Copyright © 2020 EPLA]. All rights reserved.). The spatial dimensions are in millimetres and the temperature bars in kelvin, also in the following figures. Temperature bars for frames (b) and (c) are the same as for frame (d).

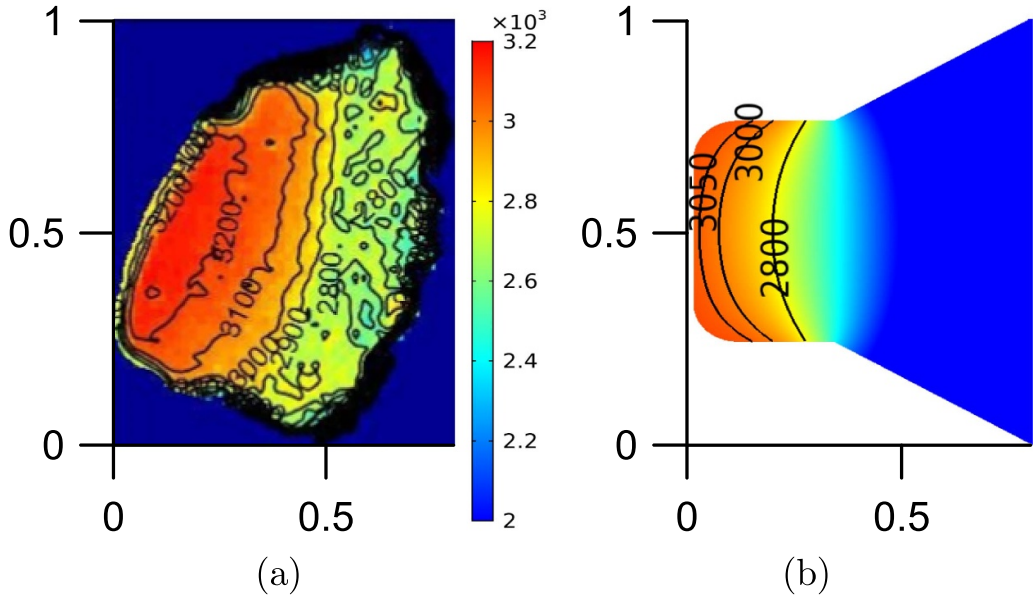

Figure 6. Distribution of temperature along the surface of the cathode tip. The insert made of W_{Th}. (a): Experiment. (b): Modelling.

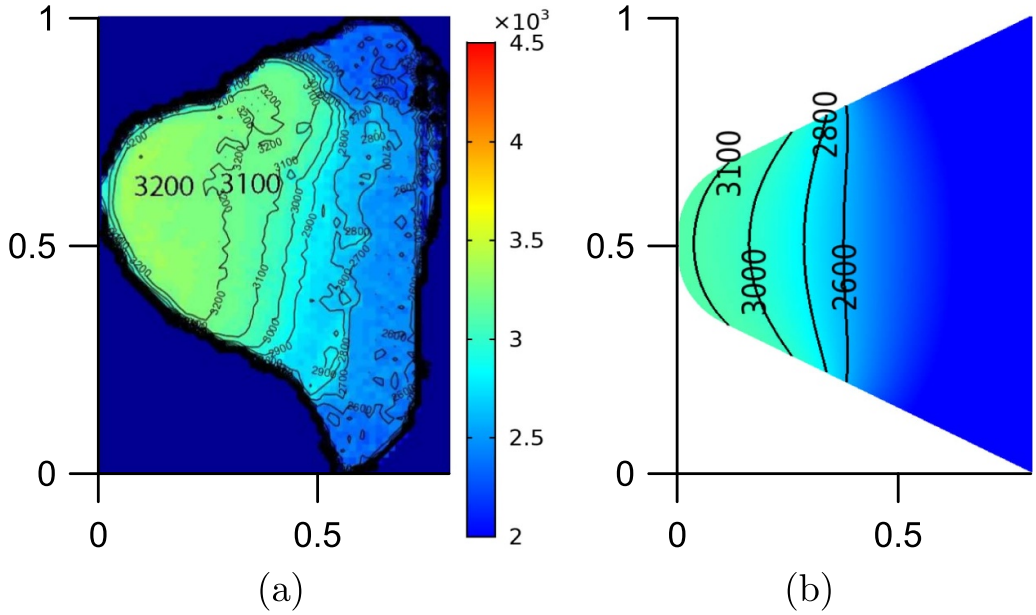

Figure 7. Distribution of temperature along the surface of the cathode tip. The insert made of W_Y. (a): Experiment. (b): Modelling.

mode, are close to each other as well. Results of modelling with the same value $A_f = 3.0$ eV are shown in figures 6(b), 7(b) and 8(b) and in table 2. Note that this value of the work function is in the spirit of previous works: it was reported for the lanthanated-tungsten arc cathode at the arc current of 200 A in [41] and is not very different from the value of 3.2 eV reported for thoriated-tungsten arc cathode at $T_w = 2900$ K in [43].

In the case of the insert made of thoriated tungsten (figure 6), the cathode tip was always in the solid phase. The tip of the cathode becomes significantly deformed during the initiation stage and the maximum temperature of the cathode tip in the stable mode is about 3200 K. The computed temperature distribution of the tip for this case presents a maximum value of 3086 K. There is a reasonably good agreement between the modelling and the experiment. For comparison, the modelling has been performed also with thermionic emission parameters for thoriated tungsten given in reference books: $A_f = 2.63$ eV, $A_{em} = 3 \times 10^4\,\mathrm{A\,m^{-2}\,K^{-2}}$; for example, these values are cited for thoriated tungsten on p. 297 of the reference book [36] and for tungsten with adsorbed electropositive layer of thorium on p 18-2 of the reference book [44].

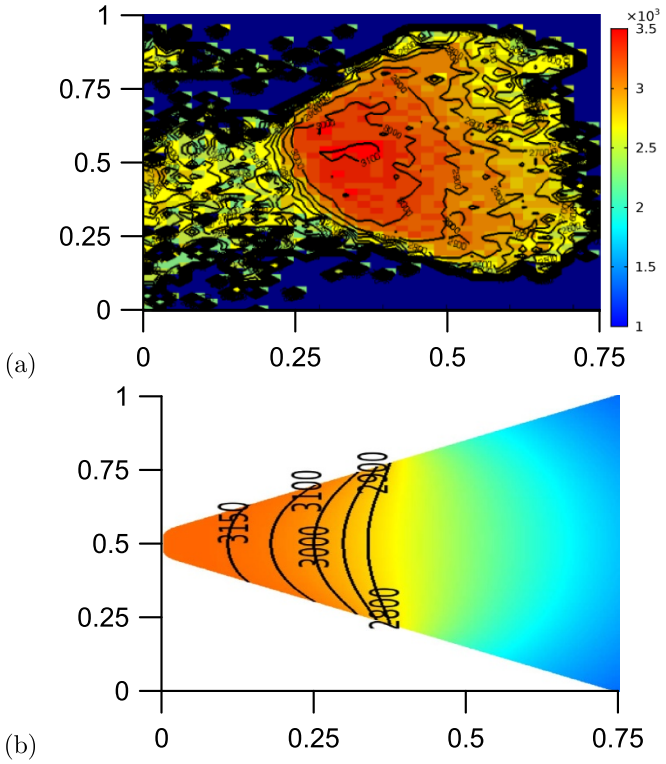

Figure 8. Distribution of temperature along the surface of the cathode tip. The insert made of W_{La}. (a): Experiment (Reproduced from [9]. [Copyright © 2015 EPLA]. All rights reserved.). The distortion of the image is due to the residual plasma glow. (b): Modelling.

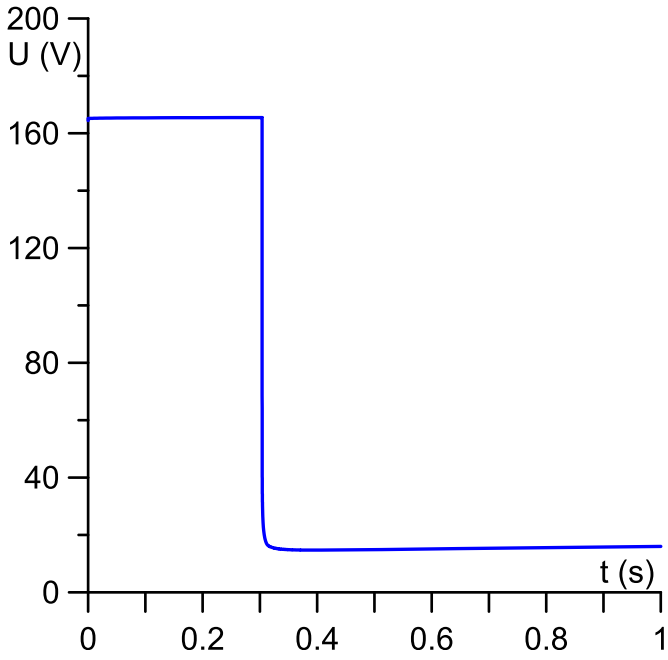

Figure 9. Evolution of the near-cathode voltage drop for the tungsten insert. Atmospheric-pressure argon plasma.

The computed maximum temperature is given in table 2 and is close to 4000 K, thus being substantially higher than the measured value. This is a clear indication that values of the work function of cold doped metal surfaces available in the literature may have little relevance for arc cathodes. Also performed was the modelling with the work function of 2.8 eV, reported for thoriated-tungsten cathode and the arc current of 200 A in the paper [41]. The computed maximum temperature is given in table 2 and is by about 300 K lower than the measured value.

In the case of the insert doped with yttrium (figure 7), the cathode material was mainly in the solid phase, but there were liquid droplets forming at its surface during the initiation stage. The maximum temperature of the tip measured in the stable mode is about 3200 K. The computed temperature distribution of the cathode tip for this case presents a maximum value of about 3115 K. There is a good agreement between measured and computed temperature distributions in this case. For comparison, also shown in table 2 are values of the maximum temperature computed with thermionic emission parameters for tungsten with adsorbed electropositive layer of yttrium taken from [44] and for tungsten doped with 1% of La_2O_3 and 1% of Y_2O_3 from [45]. The computed maximum temperatures are by, respectively, 500 and 400 K lower than the measured value.

In the case of the insert made of lanthanated tungsten (figure 8), the cathode material was never in the liquid phase during arc operation and its shape is virtually preserved. The maximum temperature of the tip of the cathode when in the stable mode of operation was recorded to be roughly 3100 K. The computed temperature distribution of the cathode tip for this case presents a maximum value of about 3160 K, in a good agreement with the measured value. For comparison, also shown in table 2 are the value of the maximum

Table 2. Measured and computed maximum temperatures of inserts made of different materials and the work function A_f and the Richardson constant A_{em} used in the modelling.

Insert material	The maximum measured temperature (K)	A_f (eV)	A_{em} (A m^{-2} K^{-2})	Reference	The maximum computed temperature (K)
W	4200	4.54	1.2×10^6	[36]	4304
W_{Th}	3200	3.0	1.2×10^6	See text	3086
		2.63	3.0×10^4	[36, 44]	3927
		2.8	1.2×10^6	[41]	2909
W_Y	3200	3.0	1.2×10^6	See text	3115
		2.7	7.0×10^4	[44]	2710
		3.71	6.9×10^7	[45]	2809
W_{La}	3100	3.0	1.2×10^6	See text	3164
		2.71	8.0×10^4	[44]	3753
		3.30	9.9×10^6	[45]	2917

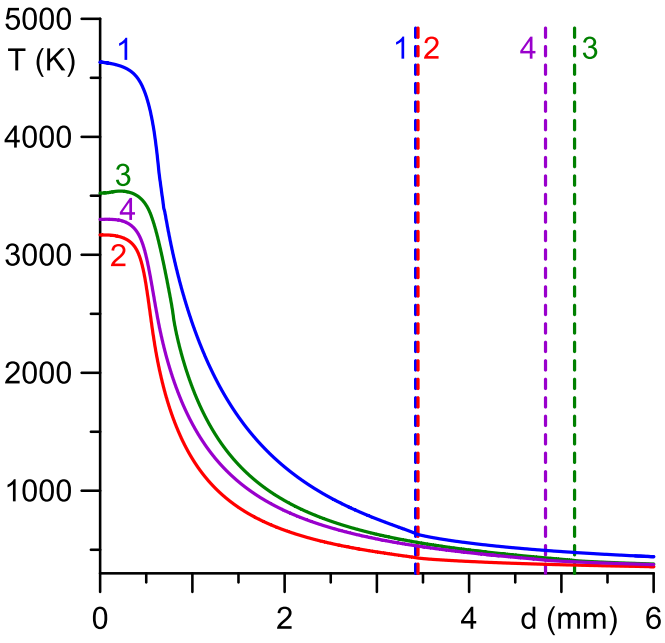

Figure 10. Distribution of temperature along the front surfaces of the insert and the copper holder for different insert materials. Dashed lines indicate the position of the point of contact of the insert and the copper holder (point *F* in figure 1). (1): pure tungsten insert. (2): W_{La}. (3): W_{Th}. (4): W_Y.

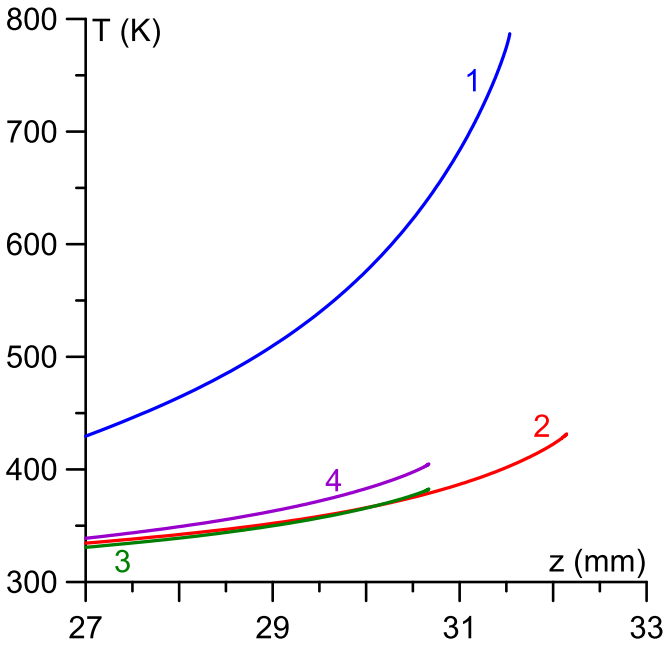

Figure 11. Distribution of temperature along the line of contact between insert and copper holder for different insert materials. (1): Pure tungsten insert. (2): W_{La}. (3): W_{Th}. (4): W_Y.

temperature computed with thermionic emission parameters for tungsten with adsorbed electropositive layer of lanthanum, taken from [44], and the value computed with thermionic emission parameters for tungsten doped with 1% of La_2O_3, taken from [45]. The former value is significantly higher that the measured one, and the latter is about 200 K lower.

Distributions of the temperature along the front surfaces of the insert and the copper holder, computed for different insert materials, are shown in figure 10. In this figure, *d* is the distance from the centre of the tip of the cathode measured along the generatrix (line *GFE* in figure 1). One can see that the temperature decreases very fast along the surface of the insert. The distribution of temperature along the line of contact between the insert and the copper holder (line *IF* in figure 1) is shown in figure 11. Note that $z = 27$ mm corresponds to the bottom of the insert (point *I* in figure 1). The temperature varies from approximately 390 K at the point *I* to 640 K at the point *F* for the insert made of pure tungsten, from 335 K to 430 K for the insert made of lanthanated tungsten, and from 340 K to 410 K for the inserts made of tungsten doped with thorium or yttrium. In all the cases, the temperature of copper is well below the melting point (we remind that the melting point of copper is 1358 K). This can be seen as an indication of a proper design of the cathode unit.

5. Concluding remarks

The modelling method based on decoupling the simulation of the cathodic part of the arc (the cathode and the near-cathode

non-equilibrium plasma layer) from the simulation of the arc on the whole has been extended to cathodes of arc plasma torches, consisting of an insert with a conical tip, made of pure or doped tungsten, and a surrounding water-cooled copper holder. The method was validated by comparison with the experiment, performed on a 200 A DC arc in atmospheric-pressure argon.

Standard work function of polycrystalline tungsten of 4.54 eV was used for modelling of pure-tungsten insert and a good agreement with the experiment was found with respect to both the insert tip shape and the temperature distribution in the tip, recorded in the stable operation mode.

There are no unambiguous data on the work function for arc cathodes made of doped tungsten, although *in situ* measurements of the effective work function of cathodes of high-pressure arc discharges reported in [40, 41] and the investigation of the effective work function of thoriated-tungsten arc cathodes reported in [43] provide some useful indications. On the other hand, the experiments of this work show that the tip temperatures of inserts made of tungsten doped with 1.5% of thorium, or lanthanum, or yttrium, recorded during the stable-mode operation at the arc current of 200 A, vary in a rather narrow range 3100–3200 K. This suggests that the work functions of doped tungsten inserts, operated in the stable mode, are close to each other as well. Indeed, results of modelling with the same value of the work function of 3.0 eV give a reasonably good agreement with the experiment in all the three cases. Note that this value is in the spirit of previous works; for example, the work functions of 2.8 and 3.0 eV were reported in [41] for tungsten cathodes doped with 2% of ThO_2 and La_2O_3, respectively, operated at the arc current of 200 A. It is interesting to note that the tip temperatures of ThO_2 and La_2O_3 cathodes reported in [41] were 3723 and 3481 K, respectively; while being higher than the values of 3100–3200 K recorded in this work (which is unsurprising given different designs of the cathodes), these values are still not too different from each other.

Data availability statement

All data that support the findings of this study are included within the article (and any supplementary files).

Acknowledgments

The work at Universidade da Madeira was supported by FCT—Fundação para a Ciência e a Tecnologia of Portugal under Projects UIDP/50010/2020 and UIDB/50010/2020 and by European Regional Development Fund through the Operational Program of the Autonomous Region of Madeira 2014–2020 under Project PlasMa-M1420-01-0145- FEDER-000016. The work at the Joint Institute for High Temperatures was supported by the Russian Science Foundation Grant No. RSF 22-29-01028. The authors are grateful to Dr H Kaufmann for the compilation of data on the emissivity of copper shown in figure 3.

ORCID iDs

M D Cunha https://orcid.org/0000-0002-0397-536X
M A Sargsyan https://orcid.org/0000-0002-7185-5765
M Kh Gadzhiev https://orcid.org/0000-0003-2935-8105
D V Tereshonok https://orcid.org/0000-0002-5188-6476
M S Benilov https://orcid.org/0000-0001-9059-1948

References

[1] Gleizes A 2015 *Plasma Chem. Plasma Process.* **35** 455
[2] Murphy A B 2015 *Plasma Chem. Plasma Process.* **35** 471
[3] Chazelas C, Trelles J P, Choquet I and Vardelle A 2017 *Plasma Chem. Plasma Process.* **37** 627
[4] Murphy A B and Uhrlandt D 2018 *Plasma Sources Sci. Technol.* **27** 063001
[5] Choquet I 2018 *Weld. World* **62** 177
[6] Benilov M S 2020 *J. Phys. D: Appl. Phys.* **53** 013002
[7] Dabringhausen L, Langenscheidt O, Lichtenberg S, Redwitz M and Mentel J 2005 *J. Phys. D: Appl. Phys.* **38** 3128
[8] Boulos M I, Fauchais P and Pfender E 2016 *Handbook of Thermal Plasmas* (Springer)
[9] Gadzhiev M K, Sargsyan M A, Tereshonok D V and Tyuftyaev A S 2015 *Europhys. Lett.* **111** 25001
[10] Gadzhiev M K, Sargsyan M A, Tereshonok D V and Tyuftyaev A S 2016 *Europhys. Lett.* **115** 35002
[11] Sargsyan M A, Tereshonok D V, Valyano G E, Scherbakov V V, Konovalov P A and Gadzhiev M K 2020 *Phys. Plasmas* **27** 023506
[12] Goryachev S V, Isakaev E H, Myasnikov M I and Chinnov V F 2008 *High Temp.* **46** 752
[13] Cagran C, Brunner C, Seifter A and Pottlacher G 2002 *High Temp.-High Press.* **34** 669
[14] Cagran C, Pottlacher G, Rink M and Bauer W 2005 *Int. J. Thermophys.* **26** 1001
[15] Sargsyan M A, Tereshonok D V, Gadzhiev M K and Tyuftyaev A S 2020 *Europhys. Lett.* **131** 45002
[16] Cunha M D, Kaufmann H T C, Santos D F N and Benilov M S 2019 *J. Phys. D: Appl. Phys.* **52** 504004
[17] Lewis R W and Ravindran K 2000 *Int. J. Numer. Methods Eng.* **47** 29
[18] Voller V R and Prakash C 1987 *Int. J. Heat Mass Transfer* **30** 1709
[19] Brent A D, Voller V R and Reid K J 1988 *Numer. Heat Transfer* **13** 297
[20] Mesyats G A and Uimanov I V 2015 *IEEE Trans. Plasma Sci.* **43** 2241
[21] Mesyats G A and Uimanov I V 2017 *IEEE Trans. Plasma Sci.* **45** 2087
[22] Kaufmann H T C, Cunha M D, Benilov M S, Hartmann W and Wenzel N 2017 *J. Appl. Phys.* **122** 163303
[23] Zhang X, Wang L, Jia S and Shmelev D L 2017 *J. Phys. D: Appl. Phys.* **50** 455203
[24] Wang L, Zhang X, Wang Y, Yang Z and Jia S 2018 *Phys. Plasmas* **25** 043511
[25] Benilov M S, Cunha M D and Naidis G V 2005 *Plasma Sources Sci. Technol.* **14** 517
[26] Santos D F N, Lisnyak M, Almeida N A, Benilova L G and Benilov M S 2021 *J. Phys. D: Appl. Phys.* **54** 195202
[27] Frohnert S and Menteln J 2022 *Contrib. Plasma Phys.* **62** e202100212
[28] Frohnert S and Mentel J 2022a *Contrib. Plasma Phys.* **62** e202100214
[29] Frohnert S and Mentel J 2022b *Contrib. Plasma Phys.* **62** e202100216
[30] Benilov M S and Cunha M D 2002 *J. Phys. D: Appl. Phys.* **35** 1736

[31] Tolias P 2017 *Nucl. Mater. Energy* **13** 42
[32] Assael M J, Kalyva A E, Antoniadis K D, Banish R M, Egry I, Wu J, Kaschnitz E and Wakeham W A 2010 *J. Phys. Chem. Ref. Data* **39** 033105
[33] White G K and Minges M L 1997 *Int. J. Thermophys.* **18** 1269
[34] Touloukian Y S, Powell R W, Ho C Y and Clemens P G 1970 *Thermal Conductivity. Metallic Elements and Alloys, Thermophysical Properties of Matter* vol 1 (IFI/Plenum)
[35] Yih S W H and Wang C T 1979 *Tungsten: Sources, Metallurgy, Properties and Applications* (Plenum Press)
[36] Fomenko V S 1981 *Emission Properties of Materials* 4th edn (Naukova Dumka) revised and supplemented, in Russian
[37] Kawano H 2008 *Prog. Surf. Sci.* **83** 1
[38] Derry G N, Kern M E and Worth E H 2015 *J. Vac. Sci. Technol.* A **33** 060801
[39] Haynes W M (ed) 2016–2017 *CRC Handbook of Chemistry and Physics* (CRC Press)
[40] Schlager W and Neiger M 2000 *J. Phys. D: Appl. Phys.* **33** 3083
[41] Tanaka M, Ushio M, Ikeuchi M and Kagebayashi Y 2005 *J. Phys. D: Appl. Phys.* **38** 29
[42] Benilov M S*et al* 2019 NCPL—On-line tool for evaluation of parameters of non-equilibrium near-cathode plasma layer in high-pressure arc plasmas (http://fisica.uma.pt/public/NCPL)
[43] Sillero J A, Ortega D, Mu noz-Serrano E and Casado E 2010 *J. Phys. D: Appl. Phys.* **43** 185204
[44] Gale W F and Totemeier T C (eds) 2004 *Smithells Metals Reference Book* 8th edn (Elsevier Butterworth-Heinemann)
[45] de Cachard J, Cadoret K, Martinez L, Veillet D and Millot F 2001 *Proc. 15th Int. Plansee Seminar* ed G Kneringer, P Roedhammer and H Wildner (Plansee Holding AG) p 574
[46] Touloukian Y S and DeWitt D P 1970 *Thermal Radiative Properties: Metallic Elements and Alloys* (*Thermophysical Properties of Matter* vol 7) (New York: IFI/Plenum)
[47] Estalote E A and Ramanathan K G 1977 *J. Opt. Soc. Am.* **67** 39
[48] Ramanathan K G and Yen S H 1977 *J. Opt. Soc. Am.* **67** 32
[49] Masuda H and Higano M 1985 *J. Opt. Soc. Am.* A **2** 1877